

# Feasible Regions for Step-Growth Melt Polycondensation Systems

Alberto Nisoli, Michael F. Doherty, and Michael F. Malone\*

Department of Chemical Engineering, University of Massachusetts, Amherst, Massachusetts 01003-3110

The attainable-region approach for reaction, mixing, and separation is applied for step-growth melt polycondensations. A concentration-based formulation is applied to develop hybrid reactor–separator models for the two-phase continuous stirred tank reactor and plug-flow reactor with simultaneous vapor removal. The evaporation of the volatile byproducts, which is typically limited by liquid-phase mass transfer, is characterized with a Thiele modulus. A reaction–separation vector that satisfies the same geometric properties as the reaction vector is defined, so that a candidate attainable region can be constructed by following a known procedure for reaction–mixing systems. The technique is demonstrated on the industrially important polycondensation step in the production of Nylon 6,6. The effect of temperature, pressure, and Thiele modulus on the candidate attainable region for number-average molecular weight is analyzed.

## Introduction and Background

Step-growth polymerization in polymer melt is a widely commercialized manufacturing process for engineering thermoplastics and synthetic fibers. In step-growth polymerization, the growth of the polymer chain occurs through the reaction of functional groups (–COOH, –OH, –CO, etc.) when the monomer has at least two functional groups. The functional groups can be located either on the same monomer molecule or on different monomers. Bifunctional monomers generate linear polymer chains. When more than two functional groups are present, the polymer molecule is either branched or cross-linked.

The overall reaction stoichiometry of step-growth polymerization can be written as



where  $P_m$  and  $P_n$  represent chains of length  $m$  and  $n$ , respectively, having two different functional groups,  $P_{m+n}$  is the resulting polymer molecule, and  $W$  is the condensation byproduct. Step-growth polymerization reactions in the melt process are reversible, and the equilibrium constant is generally not very favorable, on the order of 1 for polyesters.<sup>1</sup> Thus, to produce high molecular weight polymers, the extent of reversible reactions has to be minimized. To minimize the extent of reversible reactions, it is necessary to remove as much as possible the volatile byproducts that are formed in the forward reactions.

Typical examples of step-growth polymerization reactions include polymers such as Nylon, poly(ethylene terephthalate) (PET), and Bisphenol A polycarbonate (BPA PC). In addition to polycondensation reactions, there are also degradation reactions occurring in the last stage of the polymerization that can affect the final molecular weight as well as other important quality parameters of the final resin.

We will assume the validity of the equal reactivity hypothesis,<sup>2</sup> meaning that we will always consider forward and reverse reaction rate constants of step-growth polymerization to be independent of the chain length.

## Polycondensation Reactors

A typical continuous-melt polymerization process consists of two stages, an oligomerization stage and a polycondensation stage. In the beginning, esterification reactions dominate to convert monomers into oligomers of low molecular weight. In this stage, the viscosity of the melt is low enough that phase equilibrium can be achieved with a good agitation; thus, continuous stirred tank reactors (CSTRs) can be used. In the following stage, polycondensation reactions occur to convert low molecular weight oligomers into high molecular weight polymers. Polycondensation is typically realized in one or more finishing reactors, which are mass-transfer-limited because of the very high viscosity of the polymer melt.<sup>1</sup> The two most common types are the horizontal reactor [also called the wiped-film reactor (e.g., the reactor manufactured by Hitachi<sup>3</sup>)] and the vertical falling-film reactor (e.g., Luwa-type reactor).<sup>4</sup>

Several models of wiped-film reactors have been derived in the literature, and most of them have been applied to PET polycondensation.<sup>5</sup> Secor<sup>6</sup> used the Higbie penetration theory to represent condensation polymerization because the high viscosities suppress convection. Ault and Mellichamp<sup>7</sup> developed a model for wiped-film reactors in which the film is periodically mixed and the volatiles are removed during the film exposure time. Yokoyama et al.<sup>8</sup> from the Hitachi Research Laboratory simulated continuous polycondensation with CSTRs in series accompanied by interstage backmixing. Their model includes diffusivities and other parameters that are regressed from pilot-plant data. Amon and Denson<sup>9</sup> assumed that reaction occurs only in the bulk pool while the byproduct removal takes place only in the film. Ravindranath and Mashelkar<sup>10</sup> further developed the penetration theory model originally developed by Secor and added an analysis of axial dispersion in polycondensation reactors. They also considered the change in interfacial concentration and the influence of side reactions.<sup>11</sup> Gupta et al.<sup>12</sup> revisited the models of Amon and Denson and Ault and Mellichamp including the effect of film thickness and the unequal reactivity case for step-growth polymerization. Steppan et al.<sup>13</sup> developed a model for Nylon 6,6 polymerizers using realistic kinetic and equilibrium correlations as well as degradation reactions. Choi and co-workers did several experimental and modeling studies on melt polycon-

\* To whom correspondence should be addressed. Tel.: 413-545-0838. Fax: 413-545-1133. E-mail: mmalone@ecs.umass.edu.

denensation of PET using a screw-type reactor<sup>14</sup> and a rotating-disk reactor<sup>15,16</sup> operating under vacuum. They recently extended their analysis to forced-gas sweeping processes applied to PET<sup>17</sup> and BPA BC.<sup>18</sup> A model of an industrial PET wiped-film reactor was also developed by Bhaskar et al.<sup>19</sup> Similar models, also combined with neural network models ("hybrid models"), have been applied to an industrial reactive extrusion process for the production of Nylon 6,6.<sup>20,21</sup> Dynamic models have also been proposed to address startup and grade transition operations.<sup>22-24</sup> More recently optimization studies have been done on existing reactor models.<sup>25-27</sup>

### Reactor Models

The mass balance for polycondensation finishing reactors can be expressed using the general equation for simultaneous diffusion and chemical reaction for constant-volume systems:

$$Dc_i/Dt = D_{i,m}\nabla c_i + r_i \quad i = 1, 2, \dots, C \quad (2)$$

where  $c_i$  is the concentration [kmol/m<sup>3</sup>] of the  $i$ th species,  $D_{i,m}$  is the effective diffusivity of  $i$  in the mixture, and  $r_i$  is the production rate of the  $i$ th species [kmol/(m<sup>3</sup> s)] that can be written as

$$r_i = \sum_{j=1}^{NR} \nu_{ij} \mathcal{R}_j \quad (3)$$

where  $\mathcal{R}_j$  is the rate of the  $j$ th reaction,  $\nu_{ij}$  is the stoichiometric coefficient of the  $i$ th component in the  $j$ th reaction, and NR is the total number of chemical reactions. The first simplification of the partial differential equation (PDE) system in eq 2 is based on the assumption that the diffusion coefficient of the polymer molecules is much smaller than that of the volatile species diffusing out of the melt.<sup>6</sup> That implies that for the nonvolatile species (end groups and repeat units) the system in eq 2 can be written as

$$Dc_i/Dt = r_i \quad i = 1, 2, \dots, C - V \quad (4)$$

where  $V$  represents the number of volatile species. We will also assume that chemical reaction takes place only in the bulk and diffusion occurs only in the film. This assumption, introduced by Amon and Denson<sup>9</sup> in their model, greatly simplifies the calculations and seems to be quite reasonable. Most of the byproduct is expected to be removed from the film because of its larger surface area compared to that offered by the bulk. On the other hand, because the volume of the polymer in the film is much less than the holdup in the bulk phase, we can neglect the reaction term in the film. According to the model of Amon and Denson, we also neglect axial mixing within the pool. In the final stage of polycondensation, the amount of byproduct removed is normally very small compared to the total mass of the melt; therefore, we assume that the inlet volumetric flow rate remains constant along the reactor.

By considering an element  $dz$  along the reactor, it can be shown that the governing equation for the mass balance of the volatile species is

$$u \frac{dc_i}{dz} = r_i - k_L a (c_i - c_i^{eq}) \quad i = 1, 2, \dots, V \quad (5)$$

where  $a$  is the interfacial area per unit volume that has

units of 1/m.  $k_L a$  has units of inverse time (1/s), and  $1/k_L a$  represents a characteristic time for mass transfer. For the nonvolatile species in the melt, the mass balance is the same as that of the classical plug-flow reactor (PFR) in concentration space:

$$u \frac{dc_i}{dz} = r_i \quad i = 1, 2, \dots, C - V \quad (6)$$

We introduce two dimensionless groups, the Damköhler number ( $Da$ ) and the Thiele modulus ( $\Phi^2$ ). The Damköhler number is defined as the ratio of a characteristic residence time to a characteristic reaction time:

$$Da = t_{\text{residence}}/t_{\text{reaction}} \quad (7)$$

If  $l$  is the length of the polycondensation reactor, the residence time is  $\tau = l/u$ . In a mole fraction or activity-based rate model, the reaction rate constant always has units of inverse time regardless of the reaction order. Then we can define a characteristic reaction time as the inverse of a reaction rate constant evaluated at a reference temperature ( $1/k_{f,\text{ref}}$ ). Therefore, the Damköhler number can be expressed as

$$Da = \frac{l u}{1/k_{f,\text{ref}}} \quad (8)$$

The Thiele modulus is defined as the ratio of a characteristic diffusion time to a characteristic reaction time:

$$\Phi^2 = t_{\text{diffusion}}/t_{\text{reaction}} \quad (9)$$

We can assume the characteristic diffusion time to be the same as the characteristic time for mass transfer ( $1/k_L a$ ). The characteristic reaction time is the same as the one used in the expression of the Damköhler number. Therefore, we define the Thiele modulus as

$$\Phi^2 = \frac{1/k_L a}{1/k_{f,\text{ref}}} \quad (10)$$

Equation 5 can be expressed in terms of the dimensionless groups  $Da$  and  $\Phi^2$  and can be rewritten as

$$\frac{dc_i}{d\xi} = Da \frac{r_i}{k_{f,\text{ref}}} - \frac{Da}{\Phi^2} (c_i - c_i^{eq}) \quad i = 1, 2, \dots, V \quad (11)$$

The corresponding equation for nonvolatile species is

$$\frac{dc_i}{d\xi} = Da \frac{r_i}{k_{f,\text{ref}}} \quad i = 1, 2, \dots, C - V \quad (12)$$

The dimensionless parameters used are similar to the ones used by Stepan et al.<sup>13,28-30</sup> In the flowing film reactor model of Stepan et al.,<sup>28</sup> the PDE system of the governing equations contains a reaction term that is multiplied by  $\Phi^2$  and a separation term that is multiplied by  $\Phi^2/Da$ . In eq 11, the reaction term is multiplied by  $Da$  and the separation term by  $Da/\Phi^2$ . The reason for the apparent contradiction is that Stepan scaled the system using the diffusion time (expressed as  $H^2/D$ , where  $H$  is the film thickness and  $D$  the diffusion coefficient) as the characteristic time, while we have scaled our equations using the residence time as the characteristic time. The latter choice allows us to integrate the equations where the independent vari-

able ( $\xi$ ) always goes from 0 to 1. Also, the form of eq 11 is consistent with other formulations of reaction–separation devices,<sup>31–33</sup> as shown also in the appendix.

In analogy to the PFR case, we can write an equation of the component material balance for the CSTR using the two dimensionless parameters previously defined:

$$c_i - c_i^0 = Da \frac{r_i}{k_{f,\text{ref}}} - \frac{Da}{\Phi^2} (c_i - c_i^{\text{eq}}) \quad (13)$$

### Attainable-Region Approach

The attainable region (AR) is a geometric approach for process synthesis that addresses reactor network feasibility. The concept, first introduced by Horn,<sup>34</sup> has been extensively investigated by Hildebrandt, Glasser, and their co-workers for processes including reaction and mixing.<sup>35–40</sup> For a given system of reactions with given reaction kinetics, the AR is defined as the portion of concentration space that can be achieved from a given feed composition by any combination of reaction and mixing. This AR is sometimes called the “kinetically attainable region” to distinguish it from the “thermodynamically attainable region”, which is determined by equilibrium constraints.<sup>41</sup> Hopley et al.<sup>42</sup> looked at exothermic reversible reaction with complex kinetics, and Nicol et al.<sup>43,44</sup> included external cooling and heating systems. The AR method has also been extended to separation problems: Omtveit et al.<sup>45</sup> gave a graphical representation of reactor–separator–recycle systems in concentration space, Jobson et al.<sup>46</sup> studied the geometry of different configurations of two flash stages, Kauchali et al.<sup>47</sup> applied the AR to binary distillation, and Hausberger et al.<sup>48</sup> determined the optimal feed policy for ternary distillation systems. Feasible regions for simultaneous reaction and separation systems relevant to reactive distillation have been studied by Nisoli et al.<sup>32</sup> for cocurrent cascades of CSTRs and by Gadewar et al.<sup>49</sup> for countercurrent cascades of CSTRs. Feinberg and Hildebrandt have done extensive work on describing the mathematical properties of the AR and determining the characteristics of its boundary.<sup>50–54</sup> Lately, more research has been focused on hybrid process synthesis methods that combine the AR approach with conventional optimization techniques.<sup>55–59</sup> There have been a limited amount of applications of the AR approach to polymerization systems: Smith and Malone have extended AR methods to free-radical polymerization systems using reactor models in terms of the moments<sup>60</sup> and then included random copolymer systems.<sup>61</sup>

In this work we want to use simple CSTR and PFR reactor models to construct the convex hull for reaction–mixing melt polymerization systems. For step-growth polymerization, we calculate the candidate AR (CAR) for number-average molecular weight. For a polymer with two different end groups, the number-average molecular weight is defined as

$$M_n = \frac{2}{e_1 + e_2} \quad (14)$$

where  $e_i$  represents the moles of end group  $i$  per gram of polymer ( $e_i = c_i/\rho_m$ , where  $\rho_m$  is the mass density of the polymer melt). On the basis of eq 14, it makes more sense to keep the reactor models in concentration space to derive the CAR for  $M_n$ .

The PFR and CSTR models defined by eqs 11 and 13, respectively, can be expressed in terms of a reaction–separation vector that is always tangent to the concentration trajectory for the PFR and is collinear with the vector defined as the difference between the feed and exit concentrations for the CSTR. The reaction–separation vector can be expressed in terms of the two dimensionless parameters  $Da$  and  $\Phi^2$ :

$$dc/d\xi = R_i \quad i = 1, 2, \dots, C \quad (15)$$

$$c_i - c_i^0 = R_i \quad (16)$$

where

$$R_i = Da \frac{r_i}{k_{f,\text{ref}}} - \frac{Da}{\Phi^2} (c_i - c_i^{\text{eq}}) \quad i = 1, 2, \dots, V \quad (17)$$

is the reaction–separation vector, which is the difference of a reaction vector  $Da r_i/k_{f,\text{ref}}$  and a separation vector  $Da/\Phi^2(c_i - c_i^{\text{eq}})$ . For nonvolatile species, the reaction–separation vector reduces to the reaction vector only.

### Nylon 6,6 Polymerization

We now apply the AR approach to a typical example of step-growth polymerization such as the polyamidation reaction of Nylon 6,6:<sup>62</sup>



where an amine end group (A) reacts with a carboxyl end group (C) to form an amide linkage (L), resulting in the removal of a water molecule (W). The reaction rate constant ( $k_{\text{app}}$ ) and equilibrium constant ( $K_{\text{app}}$ ) of reaction (18) are defined in terms of mole fractions because they already account for the nonideality of the liquid mixture:

$$k_{\text{app}} = \frac{r}{x_A x_C - \frac{x_L x_W}{K_{\text{app}}}} \quad (19)$$

$$K_{\text{app}} = \left( \frac{x_L x_W}{x_A x_C} \right)_{\text{eq}} \quad (20)$$

$k_{\text{app}}$  and  $K_{\text{app}}$  will be calculated according to the activity-based model derived by Steppan et al.<sup>63</sup>

$$k_{\text{app}} = k_0 \exp \left[ -\frac{E_{\text{app}}}{R} \left( \frac{1}{T} - \frac{1}{T_0} \right) \right] \quad (21)$$

$$K_{\text{app}} = K_0 \exp \left[ -\frac{\Delta H_{\text{app}}}{R} \left( \frac{1}{T} - \frac{1}{T_0} \right) \right] \quad (22)$$

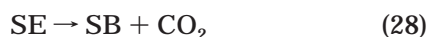
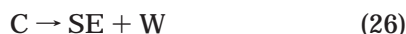
$E_{\text{app}}$  is a constant (21.400 kcal/mol).  $k_0$ ,  $K_0$ , and  $\Delta H_{\text{app}}$  depend on the mole fractions of water ( $x_W$ ) and carboxyl end group ( $x_C$ ):

$$k_0 = \exp \{ 2.55 - 0.45 \tanh [25(x_W - 0.55)] \} + 8.58 \{ \tanh [50(x_W - 0.10)] - 1 \} (1 - 30.05 x_C) \quad (23)$$

$$\Delta H_{\text{app}} = 7650 \tanh [6.5(x_W - 0.52)] + 6500 \exp(-x_W/0.065) - 800 \quad (24)$$

$$K_0 = \exp\{[1 - 0.47 \exp(-x_W^{1/2}/0.2)](8.45 - 4.2x_W)\} \quad (25)$$

Depending on the operating condition, Nylon 6,6 can be susceptible to thermal degradation, which can significantly affect product properties (changes in the number of end groups can change dyability, and small amounts of cross-linking can be detrimental during the fiber spinning process). Steppan et al.<sup>30</sup> developed a simplified kinetic model that is consistent with all of the previously published experimental data on the degradation of Nylon 6,6. The kinetic scheme includes formation of volatile species (ammonia and carbon dioxide) and considers the extent of cross-linking, according to the following reactions:



where SE refers to a stabilized (or cyclized) end group, SB to a Schiff base, and X to a cross-link. The rates of the reaction steps given by eqs 26–29 are expressed as

$$R_1 = c_T k_1 x_C \quad (30)$$

$$R_2 = c_T x_L (k_2 + k_{2C} x_A) \quad (31)$$

$$R_3 = c_T k_3 x_A x_{SE}^a \quad (32)$$

$$R_4 = c_T k_4 x_{SB}^b x_A \quad (33)$$

where  $c_T$  is the total molar concentration ( $c_T = c_A + c_C + c_L + c_W + c_{SE} + c_{SB} + c_X$ ). The kinetic parameters of the degradation model ( $k_1$ ,  $k_2$ ,  $k_{2C}$ ,  $k_3$ ,  $k_4$ ,  $a$ , and  $b$ ) are reported in Table 4 of Steppan et al.<sup>30</sup> The concentration of polymer molecules is given by

$$c_P = \frac{c_A + c_C + c_{SE} + c_{SB} - c_X}{2} \quad (34)$$

and the number-average molecular weight can be written as

$$M_n = \frac{2\rho_m}{c_A + c_C + c_{SE} + c_{SB} - c_X} \quad (35)$$

Equations 34 and 35 are valid for small amounts of cross-linking (at most, one cross-link in any polymer molecule).

**Calculation of the Initial Condition.** In the Nylon 6,6, polymerization, the initial condition of the prepolymer is given in terms of the initial number-average molecular weight ( $M_n$ ) and the initial weight fraction of water ( $\omega_W$ ) in equilibrium with the mixture. If we assume that the amine and carboxyl end groups are present in a stoichiometric amount, their concentration (in terms of moles per g of mixture) can be calculated from the definition of the number-average molecular weight:

$$e_A = e_C = 1/M_n \quad (36)$$

**Table 1. Calculation of the initial condition from  $M_n$ , wt % Water, and Temperature**

$M_n = 6200$ g/mol	$\rho = 1000$ kg/m <sup>3</sup>	water = 3.5 wt %
$e_A = 0.000161$ mol/g	$c_A = 0.161$ mol/L	$X_A = 0.0184$
$e_C = 0.000161$ mol/kg	$c_C = 0.161$ mol/L	$X_C = 0.0184$
	$c_L = 6.855$ mol/L	$X_L = 0.7807$
	$c_W = 1.603$ mol/L	$X_W = 0.1826$
$K_0 = 1418$		
$T = 553.15$ K		
$\Delta H_{app} = -7870$ cal/mol		
$K = 422.5$		

The corresponding molar concentrations  $c_A$  and  $c_C$  are derived by simply multiplying  $e_A$  and  $e_C$  by the mass density of the mixture ( $\rho_m$ ). To calculate the initial condition to use in the simulation, we can assume that at the prepolymer stage no degradation reactions have taken place yet, so that the polymer melt can be represented in terms of a four-component mixture (A, C, L, and W). The four initial mole fractions at a given temperature can be calculated by solving a nonlinear system of four equations: (1) stoichiometric equation for the mole fractions ( $x_A + x_C + x_L + x_W = 1$ ); (2) assumption that the amine and carboxyl end groups are present in a stoichiometric amount ( $x_A = x_C$ ); (3) constraint on the water mass fraction [ $f(x_A, x_C, x_L, x_W) = \omega_W$ ]; (4) chemical equilibrium constraint ( $K_{eq} = x_L x_W / x_A x_C$ ).

Once the mole fractions are known, the total concentration of the mixture can be calculated because we know the molar concentration of amine and carboxyl end groups ( $c_T = c_A/x_A$ ). Therefore, because we know all of the mole fractions and the total concentration, all of the initial concentrations can also be calculated. In all of the Nylon 6,6 calculations that will be presented, the density of the melt has been assumed to be equal to 1 g/cm<sup>3</sup>. Van Krevelen<sup>64</sup> reports a density of amorphous Nylon 6,6 of 1.07 g/cm<sup>3</sup> and a  $\Delta V_m$  (expansion due to melting) on the order of 10%, so it is reasonable to assume a melt density of approximately 1 g/cm<sup>3</sup>.

Table 1 shows an example of the calculation for a prepolymer with  $M_n = 6200$ ,  $\omega_W = 0.035$ , and  $T = 280$  °C.

## Design Procedure

Before constructing the CAR, we want to plot the maximum molecular weight that can be achieved as a function of the dimensionless parameters  $Da$  and  $\Phi^2$  for the PFR (eq 11). We assume isobaric and isothermal calculations, and we choose the reference reaction rate constant  $k_{app}^0$  as the value of the rate constant when the water and amine end-group concentrations approach zero at 200 °C ( $k_{app}^0 = 2.926$  h<sup>-1</sup>). In addition to being a useful design tool, the plots of maximum  $M_n$  as a function of  $Da$  and  $\Phi^2$  were done to check that the model makes physical sense with respect to the asymptotic behaviors (low and high  $Da$  and  $\Phi^2$ ).

We plotted a three-dimensional (3D) surface plot that is convenient for looking at asymptotic behaviors and also a contour plot that can be used for obtaining a preliminary design of wiped-film polymerizers. Contour plots have already been used by Steppan et al.,<sup>13,28</sup> so they were available to us for a qualitative comparison. An exact comparison is not possible because the Thiele modulus is defined differently and also Steppan's model is a PDE model rather than an ordinary differential equation model. Nevertheless, Steppan's diagrams were

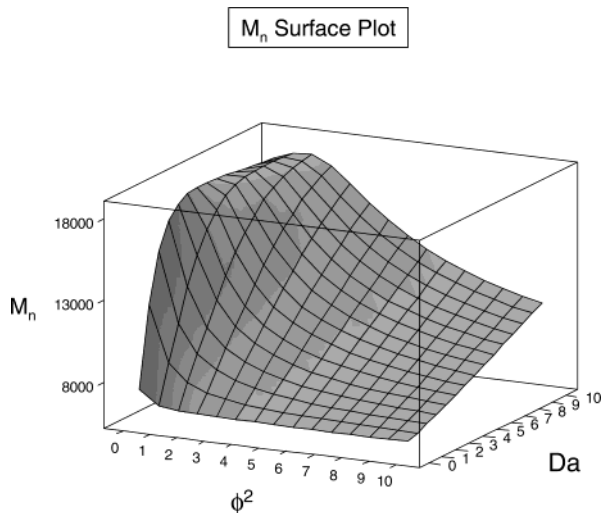


Figure 1.  $M_n$  surface plot at  $P = 300$  Torr and  $T = 280$  °C.

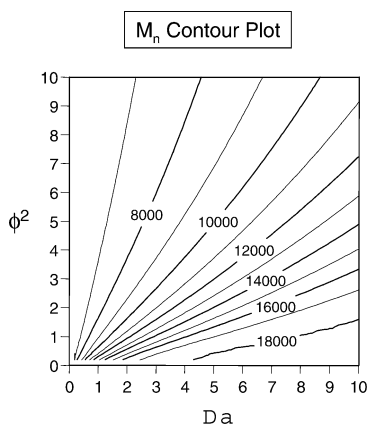


Figure 2.  $M_n$  contour plot at  $P = 300$  Torr and  $T = 280$  °C.

a good check to determine that our molecular weight values were consistent with his results.

Figure 1 shows a surface plot of  $M_n$  as a function of  $Da$  and  $\Phi^2$  for  $P = 300$  Torr,  $T = 280$  °C, and the initial composition calculated in Table 1. The model seems to predict correctly the limits of high and low values of the parameters.  $M_n$  is highest at high  $Da$  (much higher residence time compared to the characteristic reaction time, approach to reaction equilibrium) and low  $\Phi^2$  (higher rate of mass transfer and therefore fastest byproduct removal to enhance conversion).  $M_n$  is lowest at low  $Da$  (short residence times compared to reaction times) and high  $\Phi^2$  (diffusion-controlled regime and slow rate of mass transfer). The corresponding contour plot is shown in Figure 2. Notice that the contour plot can be used for a preliminary design of a wiped-film polymerizer. Once the desired outlet molecular weight has been chosen, that determines different possible combinations of the dimensionless parameters that lay on the same line at constant  $M_n$ . Every combination of  $Da$  and  $\Phi^2$  for a fixed throughput corresponds to a certain geometry of the reactor ( $l$ ), catalyst type, or concentration ( $k_{f, \text{ref}}$ ), internals giving a specific mass-transfer performance ( $k_{L,a}$ ). Alternatively, contour plots of  $M_n$  at different  $T$  and  $P$  can be used to predict the effect of a change in the operating conditions on the outlet molecular weight for an existing unit. Therefore, they serve as both a design and a simulation tool.

Figures 3 and 4 show the surface and contour plots, respectively, for  $P = 300$  Torr,  $T = 300$  °C, and the

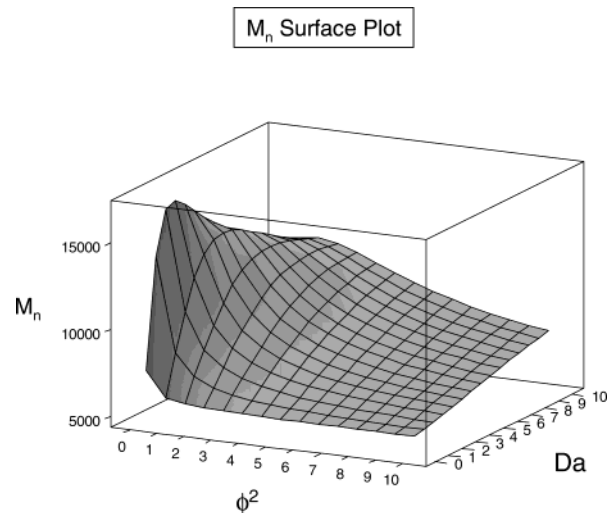


Figure 3.  $M_n$  surface plot at  $P = 300$  Torr and  $T = 300$  °C.

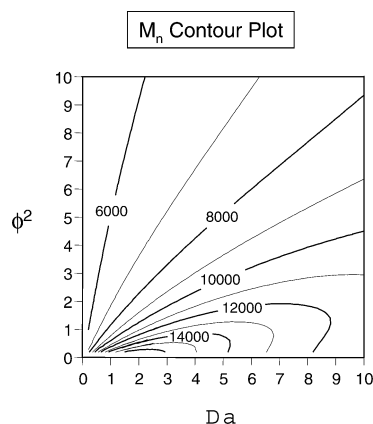


Figure 4.  $M_n$  contour plot at  $P = 300$  Torr and  $T = 300$  °C.

initial composition calculated in Table 1. As expected at higher temperature, the degradation reactions start having a significant impact on the outlet molecular weight. You can see that more clearly in the contour plot, where the curves at higher  $Da$  and lower  $\Phi^2$  show a maximum, as was already pointed out by Steppan et al.<sup>13,28</sup>

## AR Construction

For the initial condition specified in the previous section and shown in Table 1, we can construct the CAR. We assume isobaric and isothermal calculations, and as we did for the  $M_n(Da, \Phi^2)$  plots, we choose the reference reaction rate constant  $k_{\text{app}}^0$  as the value of the rate constant when the water and amine end-group concentrations approach zero at 200 °C ( $k_{\text{app}}^0 = 2.926 \text{ h}^{-1}$ ). The CAR is constructed by plotting the trajectories in the end-group concentration space ( $e_1, e_2$ ). The region in the end-group concentration space will then generate a molecular weight CAR in the ( $M_n, e_1, e_2$ ) space. Because the CAR is obtained by plotting CSTR and PFR trajectories, we need to solve the CSTR and PFR for long residence times. To get the trajectories, it is convenient to express eqs 11 and 13 in the following form:

$$\frac{dc_i}{dDa} = \frac{r_i}{k_{f, \text{ref}}} - \frac{1}{\Phi^2}(c_i - c_i^{\text{eq}}) \quad (37)$$

$$c_i - c_i^0 = \left[ \frac{r_i}{k_{f, \text{ref}}} - \frac{1}{\Phi^2}(c_i - c_i^{\text{eq}}) \right] Da \quad (38)$$

Equation 11 is equivalent to eq 37 because the following relationship applies:

$$Da \, d\xi = \frac{k_{f,\text{ref}} I \, dz}{u} = \frac{k_{f,\text{ref}} \, dz}{u} = dDa \quad (39)$$

In eqs 37 and 38,  $Da$  represents the residence time in the classical PFR and CSTR models in concentration space; therefore, the PFR and CSTR trajectories are going to be parameterized in  $Da$ .

If we neglect degradation reactions, the CAR construction becomes trivial. In that case, there are only two end groups, the amine end group ( $e_A$ ), and the carboxyl end group ( $e_C$ ). The corresponding end-group concentrations are  $c_A$  and  $c_C$ . Because no degradation reactions are considered yet,  $c_C(c_A)$  is just a straight line with slope equal to 1. Different operating conditions and parameter values will only change the length of that segment: in fact, the point at minimum end-group concentration identifies the maximum molecular weight that can be achieved, and that changes with operating conditions ( $T$ ,  $P$ ) and process parameters. That is true for both CSTR and PFR because the end groups are not volatile and the initial stoichiometric constraint is not changed by the presence of degradation reactions. The only difference between CSTR and PFR is that a certain molecular weight will be attained at different values of the residence time. The same straight line represents the CAR because no mixing lines are needed to form the convex hull in this case.

We define the CAR with respect to the number-average molecular weight ( $M_n$ ) as the surface  $M_n(c_A, c_C)$  in the  $(M_n, c_A, c_C)$  space. Because the trajectory  $c_C(c_A)$  is a straight line in the end-group concentration phase plane,  $M_n(c_A, c_C)$  is just a line in the  $(M_n, c_A, c_C)$  space.

Let us now consider the case where degradation reactions are present. When degradation is taken into account, we need to consider five end groups according to eqs 30–33; therefore, the concentration space of the end groups is a multidimensional space. To still apply the AR concept in two and three dimensions, we introduce two end-group concentrations  $c_1$  and  $c_2$  that are defined as

$$c_1 = c_A + c_C \quad (40)$$

$$c_2 = c_{SE} + c_{SB} - c_X \quad (41)$$

On the basis of eqs 40 and 41, the total concentration of polymer  $c_P$  (eq 34) and the number-average molecular weight  $M_n$  (eq 35) can be written as

$$c_P = \frac{c_1 + c_2}{2} \quad (42)$$

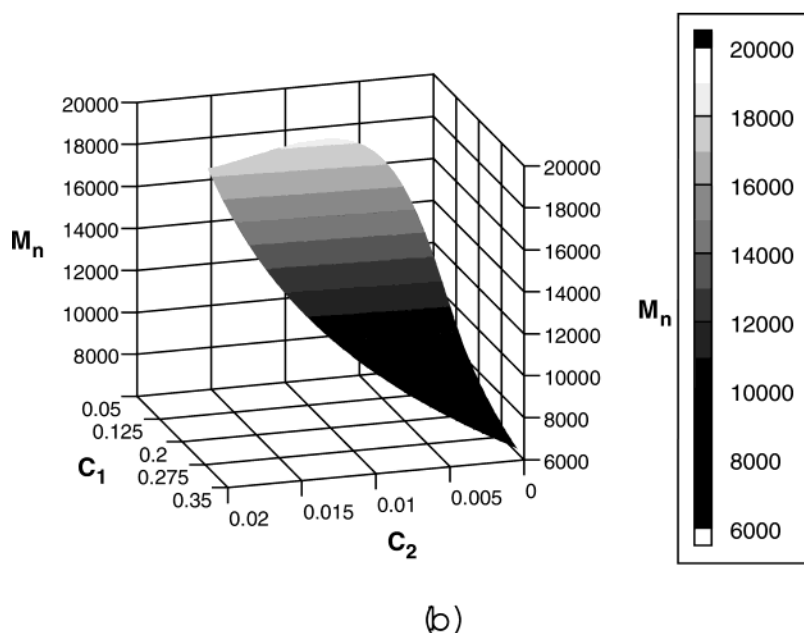
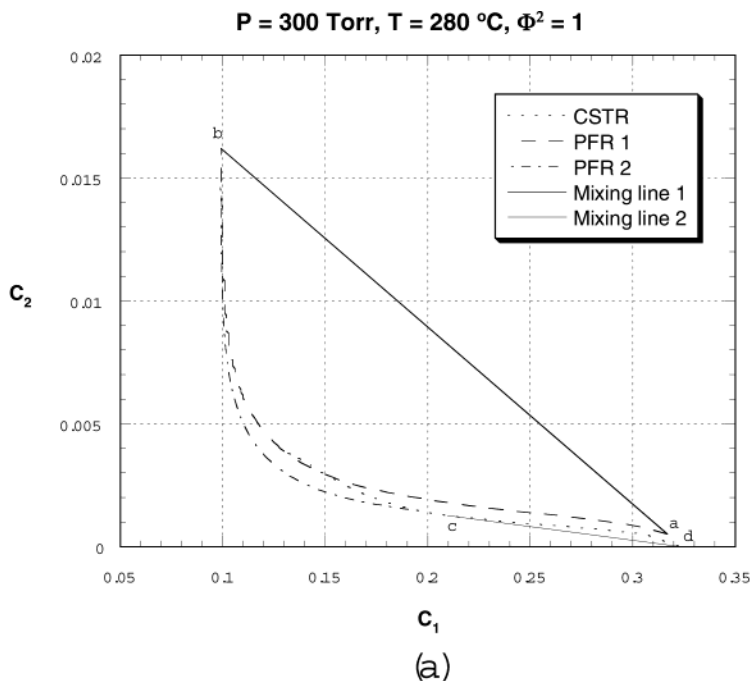
$$M_n = \frac{2\rho_m}{c_1 + c_2} \quad (43)$$

Figure 5a shows the CAR construction in the  $(c_1, c_2)$  concentration space for  $P = 300$  Torr,  $T = 280$  °C,  $\Phi^2 = 1$ , and the feed conditions calculated in Table 1 ( $T = 280$  °C and prepolymer  $M_n = 6200$  g/mol). To construct the CAR, we first plot the CSTR and PFR trajectories obtained by solving eqs 38 and 37, respectively, for large values of  $Da$ . The stopping condition for solving eqs 38 and 37 is imposed by the validity of eq 35; thus, the corresponding  $Da$  will be the value for which we have,

at most, one cross-link per polymer molecule. Because at point  $c$  in Figure 5a the reaction–separation vector points outward (as point  $c$  lies on a CSTR trajectory), we can enlarge the region by starting a PFR trajectory at that point. The region is then made convex by two mixing lines (a–b and c–d). The boundaries of the CAR are made of PFR trajectories (c–b and d–a) and mixing lines (a–b and c–d), so at every point of the region, the reaction–separation vector is either tangent or pointing inward; therefore, the region cannot be extended further. Once we constructed the CAR in the  $(c_1, c_2)$  concentration space, we can easily construct the corresponding CAR for the number-average molecular weight, which is a surface in the  $(M_n, c_1, c_2)$  3D space, according to eq 43. Figure 5b shows the CAR for  $M_n$  for  $P = 300$  Torr,  $T = 280$  °C, and  $\Phi^2 = 1$ . You can see that as the reaction between amine and carboxyl end groups proceeds along with the separation of the water byproduct ( $c_1$  becomes lower) the extent of the (irreversible) degradation reactions increases and the  $M_n$  surface goes through a maximum before the value of  $M_n$  starts decreasing as the cross-linking becomes more significant.

Now we change the operating conditions ( $P$ ,  $T$ , and  $\Phi^2$ ) and see their effect on the trajectories and the CAR. We first consider the case of increasing  $T$  and decreasing  $P$ . Both changes will produce higher conversion and a faster molecular weight build early in the reactor by lowering the water concentration in the liquid phase, although the higher temperature will also increase the rate of the degradation reactions. Figure 6a shows the CAR construction in the  $(c_1, c_2)$  concentration space for  $P = 200$  Torr,  $T = 300$  °C, and  $\Phi^2 = 1$ . We continue to use the same prepolymer conditions calculated in Table 1. As we did in the previous case, to construct the CAR, we first plot the CSTR and PFR trajectories obtained by solving eqs 38 and 37, respectively, for large values of  $Da$ . In this case the PFR starting from point d in Figure 6a and the two mixing lines (a–b and c–d) already enclose the CSTR trajectory and make a convex hull; therefore, the region cannot be extended further (another PFR trajectory is not required like in the previous case at  $P = 300$  Torr and  $T = 280$  °C). Again, once we constructed the CAR in the  $(c_1, c_2)$  concentration space, we can easily construct the corresponding 3D surface in the  $(M_n, c_1, c_2)$  space, according to eq 43. Figure 6b shows the CAR for  $M_n$  for  $P = 200$  Torr,  $T = 300$  °C, and  $\Phi^2 = 1$ . With respect to the base case analyzed before ( $P = 300$  Torr and  $T = 280$  °C), one can see that the maximum molecular weight achievable is lower because of the effect of thermal degradation, even though the same (lower) value of molecular weight can now be reached at lower  $Da$  (therefore at lower residence time, which would correspond to a shorter reactor). The higher extent of the degradation reactions in this case can also be recognized by the steeper molecular weight decay in the surface of Figure 6b.

Now we consider a change in the Thiele modulus. One interpretation of changing the Thiele modulus would be to modify the interfacial area per unit volume (e.g., by changing the type of internals of the reactor) or to change the agitation rate of the reactor blades (that would change the effective mass-transfer coefficient because the surface renewal becomes larger or smaller). In both cases, the product of the mass-transfer coefficient and interfacial area per unit volume ( $k_1 a$ ) is different and therefore changes the value of the Thiele



**Figure 5.** (a) Trajectories and CAR in concentration space at  $P = 300 \text{ Torr}$ ,  $T = 280 \text{ }^\circ\text{C}$ , and  $\Phi^2 = 1$ . (b) CAR for  $M_n$  at  $P = 300 \text{ Torr}$ ,  $T = 280 \text{ }^\circ\text{C}$ , and  $\Phi^2 = 1$ .

modulus. Figure 7a shows the CSTR and PFR trajectories. Figure 7a shows the CAR construction in the  $(c_1, c_2)$  concentration space for  $P = 300 \text{ Torr}$ ,  $T = 280 \text{ }^\circ\text{C}$ , and  $\Phi^2 = 0.2$ . After the CSTR and PFR trajectories are plotted, the region can be made convex by drawing the two mixing lines a–b and a–c. We now repeat the construction of the corresponding 3D surface in the  $(M_n, c_1, c_2)$  space, according to eq 43. Figure 7b shows the CAR for  $M_n$  for  $P = 300 \text{ Torr}$ ,  $T = 280 \text{ }^\circ\text{C}$ , and  $\Phi^2 = 0.2$ . The  $M_n$  surface for this case is very similar to the one we constructed for the base case ( $P = 300 \text{ Torr}$ ,  $T = 280 \text{ }^\circ\text{C}$ , and  $\Phi^2 = 1$ ): the maximum molecular weight has a similar value (because it is primarily determined by  $P$  and  $T$ ), and the molecular weight decay due to the degradation reactions is also comparable (the extent of the degradation reactions is mainly affected by temper-

ature). The difference between Figure 5(b) and Figure 7(b) is that the same molecular weight is achieved at very different  $Da$  number. For the case at  $\Phi^2 = 0.2$  the molecular weight build is much faster (because of the higher surface renewal due to the higher  $k_{1,a}$ ), therefore a shorter reactor (lower  $Da$ ) is required to achieve the same target molecular weight.

In Figures 5a, 6a, and 7a, the boundaries of the CAR are mixing lines or PFR trajectories where the reaction vector does not point outward. Because no CSTR inside the region can be used to reach a point in the complement of the CAR, all of the necessary conditions of the CAR in two-dimensional (2D) space are satisfied. The CAR in Figures 5a, 6a, and 7a includes a significant portion of the composition space, up to a relevant amount of degradation products. The practical range of

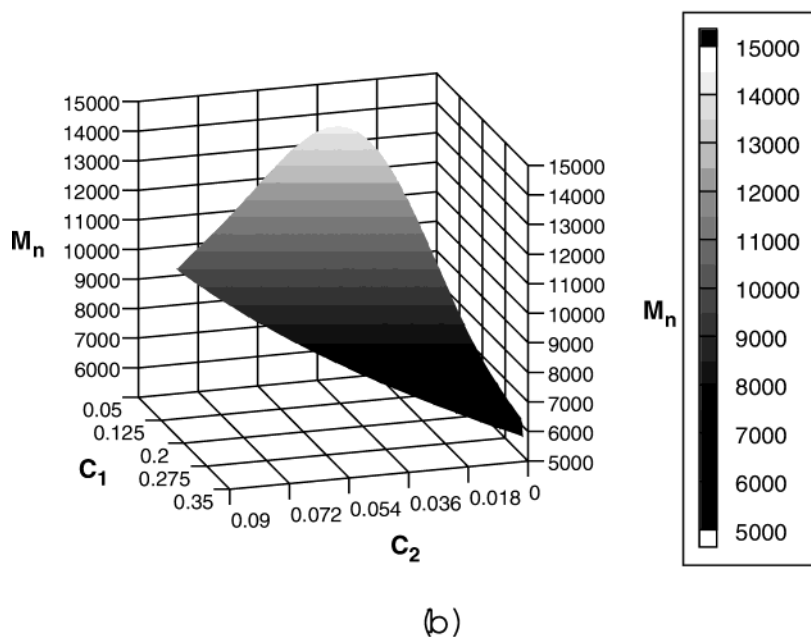
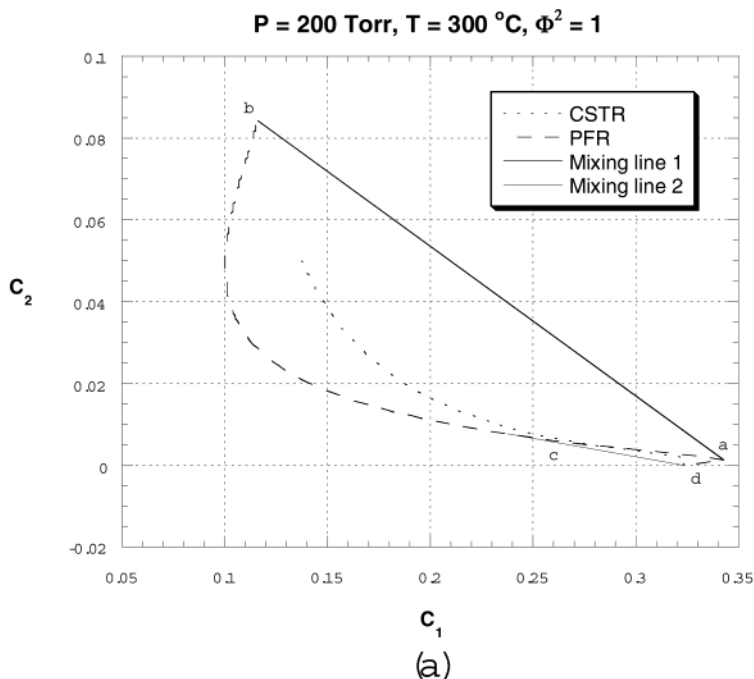


**Figure 6.** (a) Trajectories and CAR in concentration space at  $P = 200 \text{ Torr}$ ,  $T = 300 \text{ }^\circ\text{C}$ , and  $\Phi^2 = 1$ . (b) CAR for  $M_n$  at  $P = 200 \text{ Torr}$ ,  $T = 300 \text{ }^\circ\text{C}$ , and  $\Phi^2 = 1$ .

operation will be significantly smaller to ensure a target product quality, depending on the grade produced (e.g., there will be a constraint on the maximum value of  $c_2$  allowed).

### Conclusions

The AR approach for process synthesis has been applied to step-growth polycondensation systems. Reactor–separator models have been derived in concentration space for condensation polymerization reactions occurring in the liquid phase, using the end-group approach to characterize the molecular weight buildup. These models can be described in terms of two independent dimensionless parameters: the Damköhler number, which relates the residence time to the characteristic reaction time, and the Thiele modulus  $\Phi^2$ ,

which is introduced to quantify the liquid-phase mass-transfer resistance that affects the removal of the volatile byproducts.

By introduction of a reaction–separation vector, it has been shown that the reactor–separator models have the same geometric properties as the simple reactor models in concentration space. Hence, we can apply the procedure that has been previously developed for constructing the CAR.

We have studied the polycondensation of Nylon 6,6 and constructed the CAR for typical operating conditions in the end-group concentration space. If degradation reactions are not considered, the AR construction is trivial. When thermal degradation is taken into account, the CAR construction becomes a multidimensional problem because more end groups are introduced

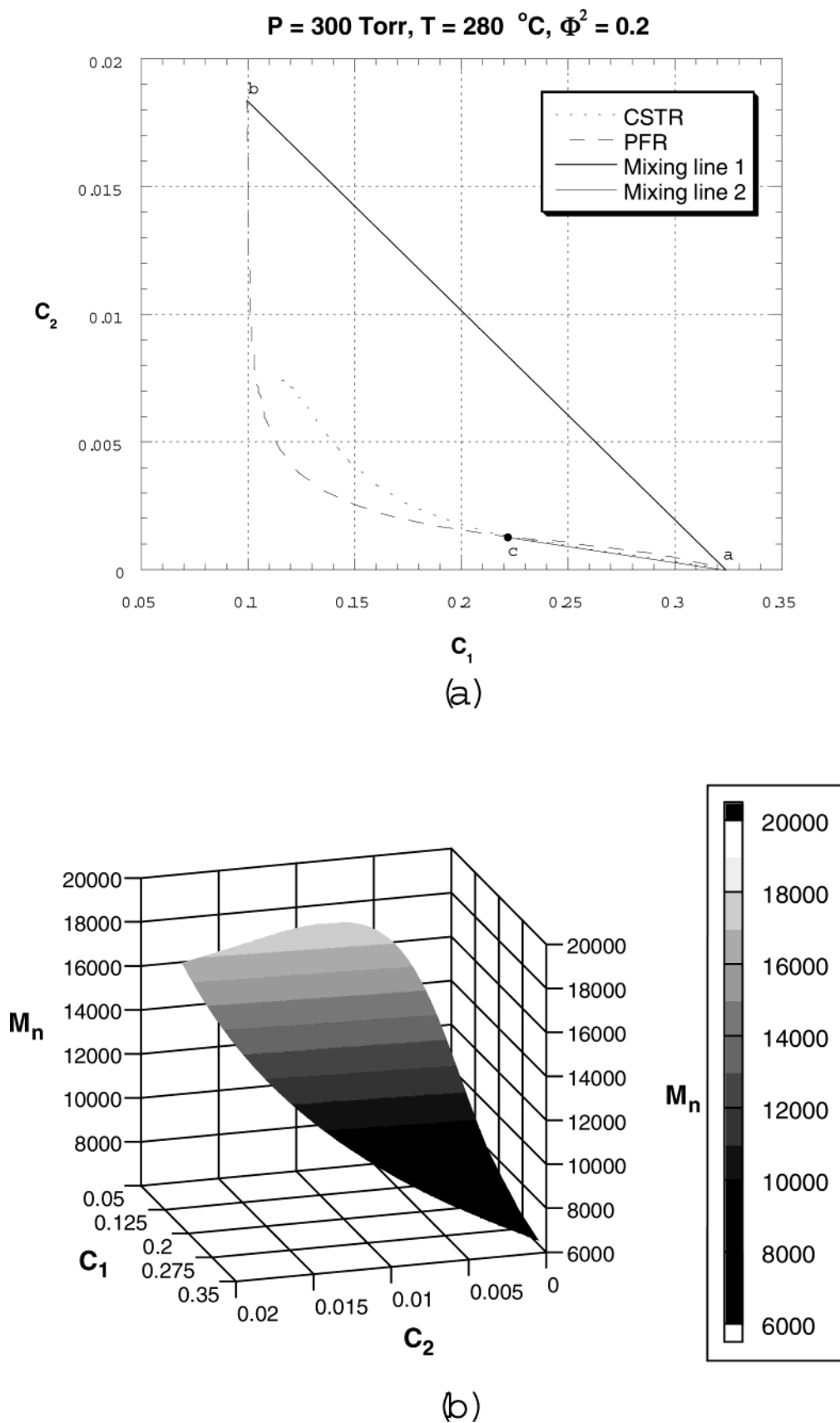


**Figure 7.** (a) Trajectories and CAR in concentration space at  $P = 300 \text{ Torr}$ ,  $T = 280 \text{ }^\circ\text{C}$ , and  $\Phi^2 = 0.2$ . (b) CAR for  $M_n$  at  $P = 300 \text{ Torr}$ ,  $T = 280 \text{ }^\circ\text{C}$ , and  $\Phi^2 = 0.2$ .

in addition to the amine and carboxyl end groups. By lumping the end groups into two concentrations, we can still reduce the problem to a 2D system in the new concentration space. Once the 2D CAR is generated, the

3D CAR for the number-average molecular weight can be easily calculated. The effect of the three main knobs in an industrial reactor ( $T$ ,  $P$ , and  $\Phi^2$ , which represents the extent of surface renewal) have been analyzed. All

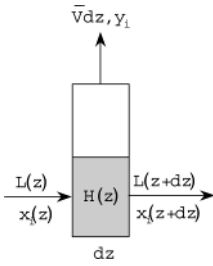


**Figure 8.** Element  $dz$  for PFR material balance.

of those three variables influence the extent and the rate of the condensation byproduct removal, hence affecting the maximum achievable molecular weight, the amount of thermal degradation, and the reactor length required for making the desired product. For this type of problem, the CAR is a convenient representation tool for choosing the optimal design (CSTR, PFR, or mixing) as well as the optimal operating parameters for attaining the target product quality.

### Appendix: Derivation of the PFR Equation from the General PFR Equation with Vapor Removal

In the work by Nisoli et al.,<sup>32</sup> the following equation was derived for a two-phase PFR where a specific vapor removal policy was applied:

$$\frac{dx_i}{d\eta} = \frac{\phi}{Da} \frac{M(\mathbf{x}_0)}{M(\mathbf{y})} (x_i - y_i) + \frac{M(\mathbf{x}_0)}{M(\mathbf{x})} \frac{k_f}{k_{f,\text{ref}}} r(\mathbf{x}) (\nu_i - \nu_T x_i) \quad (44)$$

where

$$\phi = \frac{1}{F_m} \int_0^l \bar{V}_m(z) dz \quad (45)$$

$$Da = \frac{k_{f,\text{ref}} \rho_m}{F_m} \int_0^l A(z) dz \quad (46)$$

$$d\eta \equiv \frac{M(\mathbf{x})}{M(\mathbf{x}_0)} \frac{k_{f,\text{ref}} \rho_m}{L_m(z)} A(z) dz \quad (47)$$

$M$  is the average molecular weight,  $k_{f,\text{ref}}$  is the reference reaction rate constant,  $\rho_m$  is the liquid mass density,  $L_m$  is the mass liquid rate,  $F_m$  is the mass feed rate of liquid,  $\bar{V}_m$  is the mass vapor rate per unit length,  $A$  is the cross-sectional area of the liquid.

Both eqs 5 and 44 can be derived from a general mass balance equation of a two-phase PFR. Let us consider an element  $dz$  along the reactor as shown in Figure 8. The overall mole balance across  $dz$  can be written as

$$L(z) - L(z+dz) - \bar{V} dz + \nu_T k_f r(\mathbf{x}) \rho A dz = 0 \quad (48)$$

where  $L$  is the liquid molar flow rate,  $\bar{V}$  is the molar vapor rate per unit length,  $\nu_T$  is the algebraic sum of the stoichiometric coefficients,  $k_f$  is the forward reaction rate constant,  $r$  is the driving force for the reaction (moles reacted per mole of mixture), and  $\rho$  is the molar density of the liquid. The component mole balance across  $dz$  can be expressed as

$$L(z) x_i(z) - L(z+dz) x_i(z+dz) - \bar{V} y_i dz + \nu_i k_f r(\mathbf{x}) \rho A dz = 0 \quad (49)$$

Equations 48 and 49 can be rearranged as

$$dL/dz = -\bar{V} + \nu_T k_f r(\mathbf{x}) \rho A \quad (50)$$

$$L \frac{dx_i}{dz} + x_i \frac{dL}{dz} = -\bar{V} y_i + \nu_i k_f r(\mathbf{x}) \rho A \quad (51)$$

If we substitute eq 50 into eq 51, we can obtain the general component balance equation for a two-phase PFR:

$$L \frac{dx_i}{dz} = \bar{V} (x_i - y_i) + \rho A k_f r(\mathbf{x}) (\nu_i - \nu_T x_i) \quad (52)$$

We will show how both eqs 5 and 44 can be derived from eq 52. Equation 52 can be rearranged as

$$\frac{dx_i}{dz} = \frac{\bar{V} dz}{L dz} (x_i - y_i) + \frac{k_{f,\text{ref}} \rho A}{L} \frac{k_f}{k_{f,\text{ref}}} r(\mathbf{x}) (\nu_i - \nu_T x_i) \quad (53)$$

which is equivalent to

$$\frac{L}{k_{f,\text{ref}} \rho A} \frac{dx_i}{dz} = \frac{\bar{V} dz}{L} \frac{L}{k_{f,\text{ref}} \rho A} (x_i - y_i) + \frac{k_f}{k_{f,\text{ref}}} r(\mathbf{x}) (\nu_i - \nu_T x_i) \quad (54)$$

Equation 54 can be written using mass quantities instead of molar quantities:

$$\frac{L_m}{k_{f,\text{ref}} \rho_m A} \frac{dx_i}{dz} = \frac{\bar{V}_m dz}{L_m} \frac{L_m}{k_{f,\text{ref}} \rho_m A} (x_i - y_i) + \frac{k_f}{k_{f,\text{ref}}} r(\mathbf{x}) (\nu_i - \nu_T x_i) \quad (55)$$

We can define a vapor fraction  $\phi$  and a Damköhler number  $Da$  for the element  $dz$ :

$$\phi(z) = \frac{\bar{V}_m dz}{L_m} \quad (56)$$

$$Da(z) = \frac{k_{f,\text{ref}} \rho_m A dz}{L_m} \quad (57)$$

$$\frac{\bar{V}_m dz}{L_m} \frac{L_m}{k_{f,\text{ref}} \rho_m A dz} = \frac{\phi(z)}{Da(z)} = \lim_{\Delta z_j \rightarrow dz} \frac{\phi_j}{Da_j} \quad (58)$$

where  $\phi_j$  and  $Da_j$  refer to the  $j$ th reactor in the series of CSTR used by Nisoli et al.<sup>32</sup> to approach the PFR behavior. If we assume a vapor removal policy such that

$$\frac{\phi(z)}{Da(z)} = \text{constant} = \frac{\int_0^l \bar{V}_m(z) dz}{F_m} \frac{F_m}{k_{f,\text{ref}} \rho_m \int_0^l A(z) dz} = \frac{\phi}{Da} \quad (59)$$

Equation 55 can be written as

$$\frac{L_m}{k_{f,\text{ref}}\rho_m A} \frac{dx_i}{dz} = \frac{\phi}{Da} \frac{M(\mathbf{x})}{M(\mathbf{y})} (x_i - y_i) + \frac{k_f}{k_{f,\text{ref}}} r(\mathbf{x}) (\nu_i - \nu_T x_i) \quad (60)$$

If we multiply the left- and right-hand sides of eq 60 by the ratio  $M(\mathbf{x}_0)/M(\mathbf{x})$ , eq 60 is equivalent to eq 44.

In the case of wiped-film polymerizers, it is more convenient to start the derivation from the general equation (52) in the following form:

$$d(Lx_i)/dz = -\bar{V}y_i + \nu_i k_{fr}(\mathbf{x}) \rho A \quad (61)$$

The vapor rate of volatile component  $i$  per unit length ( $\bar{V}y_i$ ) can be expressed using the molar flux of component  $i$  diffusing from the polymer melt:

$$\bar{V}y_i = k_L a \rho A (x_i - x_i^{\text{eq}}) \quad (62)$$

Therefore, eq 61 can be written as

$$d(Lx_i)/dz = \nu_i k_{fr}(\mathbf{x}) \rho A - k_L a \rho A (x_i - x_i^{\text{eq}}) \quad (63)$$

Because  $L = Q\rho$  ( $Q$  = volumetric flow rate), eq 63 is equivalent to

$$d(Q\rho x_i)/dz = \nu_i k_{fr}(\mathbf{x}) \rho A - k_L a \rho (x_i - x_i^{\text{eq}}) A \quad (64)$$

Because for wiped-film polymerizers the amount of vapor removed is very small compared to the liquid flow rate of the polymer melt, the volumetric flow rate can be considered constant and taken out of the derivative. Also, by considering that  $r_i = \nu_i k_{fr}(\mathbf{x}) \rho$  and  $c_i = \rho x_i$ , eq 64 can be rewritten as

$$Q \frac{dc_i}{dz} = r_i A - k_L a (c_i - c_i^{\text{eq}}) A \quad (65)$$

If we divide the left- and right-hand sides of eq 65 by the area  $A$ , eq 65 becomes

$$u \frac{dc_i}{dz} = r_i - k_L a (c_i - c_i^{\text{eq}}) \quad (66)$$

where  $u$  is the average velocity of the melt. Equation 66 is the same as eq 5.

## Notation

$a$  = interfacial area per unit volume, 1/m  
 $c_i$  = concentration of component  $i$ , kmol/m<sup>3</sup>  
 $c_i^{\text{eq}}$  = equilibrium concentration of component  $i$  at the interface, kmol/m<sup>3</sup>  
 $C$  = total number of components  
 $D_{i,m}$  = effective diffusivity of component  $i$  in a mixture, cm<sup>2</sup>/s  
 $Da$  = first Damköhler number  
 $e_i$  = moles of end group  $i$  per gram of polymer, mol/g  
 $E_{\text{app}}$  = apparent activation energy, kcal/mol  
 $F$  = feed flow rate, kmol/s  
 $\Delta H_{\text{app}}$  = apparent enthalpy of reaction, kcal/mol  
 $k_0$  = preexponential factor, 1/s  
 $k_{\text{app}}^0$  = apparent reaction rate constant, 1/s  
 $k_{\text{app}}^{\text{ref}}$  = reference reaction rate constant, 1/s  
 $k_{f,\text{ref}}$  = forward reaction rate constant at the reference temperature, 1/s  
 $k_L$  = mass-transfer coefficient, m/s

$K_0$  = reference equilibrium constant  
 $K_{\text{app}}$  = apparent reaction equilibrium constant  
 $K_{\text{eq}}$  = reaction equilibrium constant  
 $l$  = length of the reactor, m  
 $L$  = liquid molar flow rate, kmol/s  
 $M_n$  = number-average molecular weight, g/mol  
 $M(\mathbf{x})$  = average molecular weight ( $=\sum_{i=1}^C M_i x_i$ )  
 $N_i$  = molar flux of component  $i$ , kmol/(m<sup>2</sup> s)  
 $NR$  = total number of chemical reactions  
 $P$  = system pressure, Pa  
 $Q$  = volumetric flow rate, m<sup>3</sup>/s  
 $r(\mathbf{x})$  = driving force for the reaction, moles reacted per mole of mixture  
 $r_i$  = rate of production for component  $i$ , kmol/(m<sup>3</sup> s)  
 $R$  = universal gas constant, 8.3145 kJ/(mol K)  
 $R_i$  = reaction-separation vector, kmol/m<sup>3</sup>  
 $\mathcal{R}_j$  = rate of reaction  $j$ , kmol/(m<sup>3</sup> s)  
 $t$  = time, s  
 $T$  = temperature, °C  
 $u$  = mean velocity of the melt, m/s  
 $\bar{V}$  = molar vapor rate per unit length, kmol/(m s)  
 $\mathbf{x}$  = state vector  
 $x_i$  = mole fraction of component  $i$  in the liquid phase  
 $y_i$  = mole fraction of component  $i$  in the vapor phase  
 $z$  = axial coordinate in a PFR, m

## Greek Letters

$\eta$  = dimensionless time  
 $\nu_i$  = stoichiometric coefficient of component  $i$   
 $\nu_T$  = summation of all stoichiometric coefficients  
 $\rho$  = molar density, kmol/m<sup>3</sup>  
 $\rho_m$  = mass density, kg/m<sup>3</sup>  
 $\phi$  = vapor fraction  
 $\Phi^2$  = Thiele modulus (square)  
 $\xi$  = dimensionless time

## Subscripts and Superscripts

0 = initial condition, reference condition  
 $A$  = amine end group  
 $\text{app}$  = apparent  
 $C$  = carboxyl end group  
 $i$  = component index  
 $j$  = reaction index  
 $L$  = liquid phase  
 $L$  = amide linkage  
 $m$  = mass-based quantity  
 $n$  = number average  
 $\text{ref}$  = reference  
 $SB$  = Schiff base end group  
 $SE$  = stabilized end group  
 $T$  = total  
 $W$  = water  
 $X$  = cross-link

## Literature Cited

- (1) Gupta, S. K.; Kumar, A. *Reaction Engineering of Step Growth Polymerization*; Plenum Press: New York, 1987.
- (2) Flory, P. J. *Principles of Polymer Chemistry*, 1st ed.; Cornell University Press: Ithaca, NY, 1953.
- (3) Kinoshita, T.; Harada, K.; Motohiro, S. U.S. Patent 6,329,495, 2001.
- (4) Bechtler, H. C. U.S. Patent 3,107,194, 1963.
- (5) Ravindranath, K.; Mashelkar, R. A. Polyethylene Terephthalate—II. Engineering Analysis. *Chem. Eng. Sci.* **1986**, *41*, 2969.
- (6) Secor, R. M. The Kinetics of Condensation Polymerization. *AIChE J.* **1969**, *15*, 861.
- (7) Ault, J. W.; Mellichamp, D. A Diffusion and Reaction Model for Simple Polycondensation. *Chem. Eng. Sci.* **1972**, *27*, 1441.
- (8) Yokoyama, H.; Sano, T.; Chijiwa, T.; Kajiya, R. A Simulation Method for Ethylene Glycol Terephthalate Polycondensation Process. *J. Jpn. Pet. Inst.* **1978**, *21*, 271.

- (9) Amon, M.; Denson, C. D. Simplified Analysis of the Performance of Wiped-Film Polycondensation Reactors. *Ind. Eng. Chem. Fundam.* **1980**, *19*, 415.
- (10) Ravindranath, K.; Mashelkar, R. A. Modeling of Poly-(Ethylene Terephthalate) Reactors: 6. A Continuous Process for Final Stages of Polycondensation. *Polym. Eng. Sci.* **1982**, *22*, 628.
- (11) Ravindranath, K.; Mashelkar, R. A. Finishing Stages of PET Synthesis: a Comprehensive Model. *AIChE J.* **1984**, *30*, 415.
- (12) Gupta, S. K.; Kumar, A.; Ghosh, A. K. Simulation of Reversible AA + B'B' Polycondensations in Wiped Film Reactors. *J. Appl. Polym. Sci.* **1983**, *28*, 1063.
- (13) Steppan, D. D.; Doherty, M. F.; Malone, M. F. Wiped Film Reactor Model for Nylon 6,6 Polymerization. *Ind. Eng. Chem. Res.* **1990**, *29*, 2012.
- (14) Laubriet, C.; LeCorre, B.; Choi, K. Y. Two-Phase Model for Continuous Final Stage Melt Polycondensation of Poly(ethylene terephthalate). 1. Steady-State Analysis. *Ind. Eng. Chem. Res.* **1991**, *30*, 2.
- (15) Cheong, S. I.; Choi, K. Y. Melt polycondensation of poly(ethylene terephthalate) in a rotating disk reactor. *J. Appl. Polym. Sci.* **1995**, *58*, 1473.
- (16) Cheong, S. I.; Choi, K. Y. Modeling of a continuous rotating disk polycondensation reactor for the synthesis of thermoplastic polyesters. *J. Appl. Polym. Sci.* **1996**, *61*, 763.
- (17) Woo, B.; Choi, K. Y.; Goranov, K. The forced gas sweeping process for semibatch melt polycondensation of poly(ethylene terephthalate). *J. Appl. Polym. Sci.* **2001**, *81*, 1388.
- (18) Woo, B.; Choi, K. Y.; Song, K. H. Melt polycondensation of bisphenol A polycarbonate by forced gas sweeping process. II. Continuous rotating-disk reactor. *Ind. Eng. Chem. Res.* **2001**, *40*, 3459.
- (19) Bhaskar, V.; Gupta, S. K.; Ray, A. K. Modeling of an industrial wiped film poly(ethylene terephthalate) reactor. *Polym. React. Eng.* **2001**, *9*, 71.
- (20) Giudici, R.; Oller Do Nascimento, C. A.; Capocchi Beiler, I.; Scherbakoff, N. Modeling of Industrial Nylon-6,6 Polycondensation Process in a Twin-Screw Extruder Reactor. I. Phenomenological Model and Parameter Adjusting. *J. Appl. Polym. Sci.* **1998**, *67*, 1573.
- (21) Oller Do Nascimento, C. A.; Giudici, R.; Scherbakoff, N. Modeling of industrial nylon-6,6 polymerization process in a twin-screw extruder reactor. II. Neural networks and hybrid model. *J. Appl. Polym. Sci.* **1999**, *72*, 905.
- (22) Castres Saint Martin, H.; Choi, K. Y. Two-phase model for continuous final-stage melt polycondensation of poly(ethylene terephthalate). 2. Analysis of dynamic behavior. *Ind. Eng. Chem. Res.* **1991**, *30*, 1712.
- (23) Lei, G. D.; Cheong, S. I.; Choi, K. Y. Modeling and control of continuous melt polycondensation reactors for the synthesis of thermoplastic polymers. *IFAC Symp. Ser.* **1993**, *2*, 167.
- (24) Hipp, A. K.; Ray, W. H. A Dynamic Model for Condensation Polymerization in Tubular Reactors. *Chem. Eng. Sci.* **1996**, *51*, 281.
- (25) Bhaskar, V.; Gupta, S. K.; Ray, A. K. Multiobjective optimization of an industrial wiped-film PET reactor. *AIChE J.* **2000**, *46*, 1046.
- (26) Bhaskar, V.; Gupta, S. K.; Ray, A. K. Applications of multiobjective optimization in chemical engineering. *Rev. Chem. Eng.* **2000**, *16*, 1.
- (27) Ha, K.; Rhee, H. Optimal reaction conditions for the minimization of energy consumption and by-product formation in a poly(ethylene terephthalate) process. *J. Appl. Polym. Sci.* **2002**, *86*, 993.
- (28) Steppan, D. D.; Doherty, M. F.; Malone, M. F. A Flowing Film Model for Continuous Nylon 6,6 Polymerization. *Ind. Eng. Chem. Res.* **1989**, *28*, 1324.
- (29) Steppan, D. D.; Doherty, M. F.; Malone, M. F. Film Diffusion Effects in Nylon 6,6 Polymerization. *J. Appl. Polym. Sci.* **1990**, *39*, 603.
- (30) Steppan, D. D.; Doherty, M. F.; Malone, M. F. A Simplified Degradation Model for Nylon 6,6 Polymerization. *J. Appl. Polym. Sci.* **1991**, *42*, 1009.
- (31) Venimadhavan, G.; Malone, M. F.; Doherty, M. F. Effect of Kinetics on Residue Curve Maps for Reactive Distillation. *AIChE J.* **1994**, *40*, 1814. Correction: *AIChE J.* **1995**, *41*, 2613.
- (32) Nisoli, A.; Malone, M. F.; Doherty, M. F. Attainable Regions for Reaction with Separation. *AIChE J.* **1997**, *43*, 374.
- (33) Venimadhavan, G.; Malone, M. F.; Doherty, M. F. Bifurcation study of kinetic effects in reactive distillation. *AIChE J.* **1999**, *45*, 546.
- (34) Horn, F. Attainable and nonattainable regions in chemical reaction technique. *Third European Symposium on "Chemical Reaction Engineering"*; Pergamon Press: New York, 1964; p 293.
- (35) Glasser, D.; Hildebrandt, D.; Crowe, C. A Geometric Approach to Steady Flow Reactors: The Attainable Region and Optimization in Concentration Space. *Ind. Eng. Chem. Res.* **1987**, *26*, 1803.
- (36) Hildebrandt, D.; Glasser, D. The Attainable Region and Optimal Reactor Structures. *Chem. Eng. Sci.* **1990**, *45*, 2161.
- (37) Hildebrandt, D.; Glasser, D.; Crowe, C. Geometry of the Attainable Region Generated by Reaction and Mixing: With and without Constraints. *Ind. Eng. Chem. Res.* **1990**, *29*, 49.
- (38) Glasser, B.; Hildebrandt, D.; Glasser, D. Optimal Mixing for Exothermic Reversible Reactions. *Ind. Eng. Chem. Res.* **1992**, *31*, 1541.
- (39) Glasser, D.; Hildebrandt, D.; Godorr, S. The Attainable Region for Segregated, Maximum Mixed, and Other Reactor Models. *Ind. Eng. Chem. Res.* **1994**, *33*, 1136.
- (40) Godorr, S. A.; Hildebrandt, D.; Glasser, D. The attainable region for systems with mixing and multiple-rate processes: finding optimal reactor structures. *Chem. Eng. J.* **1994**, *54*, 175.
- (41) Shinnar, R.; Feng, C. A. Structure of Complex Catalytic Reactions: Thermodynamic Constraints in Kinetic Modeling and Catalyst Evaluation. *Ind. Eng. Chem. Fundam.* **1985**, *24*, 153.
- (42) Hopley, F.; Glasser, D.; Hildebrandt, D. Optimal reactor structures for exothermic reversible reactions with complex kinetics. *Chem. Eng. Sci.* **1996**, *51*, 2399.
- (43) Nicol, W.; Hildebrandt, D.; Glasser, D. Process synthesis for reaction systems with cooling via finding the attainable region. *Comput. Chem. Eng.* **1997**, *21*, S35.
- (44) Nicol, W.; Hernier, M.; Hildebrandt, D.; Glasser, D. The attainable region and process synthesis: reaction systems with external cooling and heating. The effect of relative cost of reactor volume to heat exchange area on the optimal process layout. *Chem. Eng. Sci.* **2001**, *56*, 173.
- (45) Omtveit, T.; Tanskanen, J.; Lien, K. Graphical Targeting Procedures for Reactor Systems. *Comput. Chem. Eng.* **1994**, *18*, S113.
- (46) Jobson, M.; Hildebrandt, D.; Glasser, D. Attainable products for the vapour-liquid separation of homogeneous ternary mixtures. *Chem. Eng. J.* **1995**, *59*, 51.
- (47) Kauchali, M.; McGregor, C.; Hildebrandt, D. Binary distillation re-visited using the attainable region theory. *Comput. Chem. Eng.* **2000**, *24*, 231.
- (48) Hausberger, B.; Hildebrandt, D.; Glasser, D.; McGregor, C. Feed addition policies for ternary distillation columns. *AIChE Symp. Ser.* **2000**, *323*, 402.
- (49) Gadewar, S.; Malone, M. F.; Doherty, M. F. Feasible region for a countercurrent cascade of vapor-liquid CSTRs. *AIChE J.* **2002**, *48*, 800.
- (50) Feinberg, M.; Hildebrandt, D. Optimal reactor design from a geometric viewpoint—I. Universal properties of the attainable region. *Chem. Eng. Sci.* **1997**, *52*, 1637.
- (51) Feinberg, M. Recent results in optimal reactor synthesis via attainable region theory. *Chem. Eng. Sci.* **1999**, *54*, 2535.
- (52) Feinberg, M. Optimal reactor design from a geometric viewpoint. Part II. Critical sidestream reactors. *Chem. Eng. Sci.* **2000**, *55*, 2455.
- (53) Feinberg, M. Optimal reactor design from a geometric viewpoint—III. Critical CFSTRs. *Chem. Eng. Sci.* **2000**, *55*, 3553.
- (54) Feinberg, M. Toward a Theory of Process Synthesis. *Ind. Eng. Chem. Res.* **2002**, *41*, 3751.
- (55) Pahor, B.; Irsic, N.; Kravanja, Z. MINLP synthesis and modified attainable region analysis of reactor networks in overall process schemes using more compact reactor superstructure. *Comput. Chem. Eng.* **2000**, *24*, 1403.
- (56) Rooney, W. C.; Hausberger, B. P.; Biegler, L. T.; Glasser, D. Convex attainable region projections for reactor network synthesis. *Comput. Chem. Eng.* **2000**, *24*, 225.
- (57) Rooney, W. C.; Biegler, L. T. Multiperiod reactor network synthesis. *Comput. Chem. Eng.* **2000**, *24*, 2055.
- (58) Burri, J. F.; Wilson, S. D.; Manousiouthakis, V. I. Infinite Dimensional State-space approach to reactor network synthesis: application to attainable region construction. *Comput. Chem. Eng.* **2002**, *26*, 849.

(59) Kauchali, M.; Rooney, W. C.; Biegler, L. T.; Glasser, D.; Hildebrandt, D. Linear programming formulations for attainable region analysis. *Chem. Eng. Sci.* **2002**, *57*, 2015.

(60) Smith, R. L.; Malone, M. F. Attainable Regions for Polymerization Reaction Systems. *Ind. Eng. Chem. Res.* **1997**, *36*, 1076.

(61) Smith, R. L.; Malone, M. F. Feasible compositions for random copolymerizations. *Polym. Eng. Sci.* **2001**, *41*, 145.

(62) Jaswal, I.; Pugi, K. U.S. Patent 3,900,450, 1975.

(63) Steppan, D. D.; Doherty, M. F.; Malone, M. F. A Kinetic and Equilibrium Model for Nylon 6,6 Polymerization. *J. Appl. Polym. Sci.* **1987**, *33*, 2333.

(64) Van Krevelen, D. W. *Properties of Polymers*, 2nd ed.; Elsevier Scientific Publishing Co.: Amsterdam, The Netherlands, 1976.

*Received for review* March 4, 2003

*Revised manuscript received* September 18, 2003

*Accepted* September 29, 2003

IE030220W